Journal of Magnetic Resonance **143,** 280–291 (2000)
doi:10.1006/jmre.1999.1988, available online at http://www.idealibrary.com on IDEAL®

Refocused Primary Echo: A Zero Dead Time Detection of the Electron Spin Echo Envelope Modulation

A. V. Astashkin[1,2] and A. M. Raitsimring

Department of Chemistry, University of Arizona, Tucson, Arizona 85721-0041

Received June 23, 1999; revised November 17, 1999

We report on the two-dimensional (2D) implementation of the refocused primary electron spin echo envelope modulation (ESEEM) technique, its theory and experimental application to a model system and a system of biological interest. This technique is virtually free of dead time along one time coordinate. The ESEEM obtained by integration of the 2D time-domain data of the refocused primary ESEEM over one of the time coordinates shows the intensity of the sum combination harmonics proportional to k^2 for $k \ll 1$ and proportional to k for $k \sim 1$ (k is a usual notation for the modulation amplitude factor). This feature, in combination with the adjustment of k by means of variation of the operational frequency of the spectrometer, was found to be very useful for detection of protons with distributed hyperfine interaction parameters situated close to the electron spin. © 2000 Academic Press

Key Words: **ESE; ESEEM; dead time; sum combination line; matrix line suppression.**

INTRODUCTION

While investigating the structure of biological systems by electron spin echo envelope modulation (ESEEM) spectroscopy, one often encounters a situation in which the positions of the protons close to the electron spin are distributed rather than unique. This structural inhomogeneity leads to a distribution of the hyperfine interactions (hfi) and may well result in a decrease of the intensities of the ESEEM spectral lines below detection limits. One of the most important reasons for this intensity drop is related to a spectrometer dead time, which, unless special technical measures are undertaken, usually amounts to 100–150 ns. In many cases it does not result in any problem because the damping of the ESEEM harmonics, even in orientationally disordered systems, may be sufficiently long (*1*). However, in a case of a broad and smooth hfi distribution, the ESEEM harmonics may decay within the dead time and escape detection. The problem is further aggravated by a presence of distant matrix protons (e.g., from protein backbone) that give intense lines obscuring the observation of what has remained from the desired lines of close protons after the dead time.

Several direct technical approaches to reduce the spectrometer dead time have been reported (*2–6*). Also, the suppression of unwanted matrix lines can, in principle, be achieved with a complete isotopic substitution of protons in protein backbone. Alternatively, these problems can be addressed using the dead time-free pulse sequences (*7–9*) and employing, e.g., the blind spots arising in most multipulse techniques to suppress the unwanted ESEEM harmonics. In this work we discuss an example of a zero dead time technique based on refocusing of the primary echo signal, which allows one to suppress the sum combination line due to distant matrix protons in a different way, utilizing the accentuated nonlinearity of the dependence of the ESEEM amplitude on the hfi. Other examples of using refocusing of the ESE signal, though related to pulsed electron-nuclear double resonance rather than to the ESEEM, can be found in Refs. (*10, 11*).

The refocusing of the two-pulse ESE signal was proposed by Grupp *et al.* (*12*) for reducing the dead time in the primary ESEEM experiment. In the original work (*12*), the technique was introduced as one-dimensional (1D) because the refocused ESEEM was implicitly assumed to be same as the usual primary ESEEM. Here we show that this technique is essentially two-dimensional (2D). We present its theory and implementation, and demonstrate some properties of this technique differing it from the primary ESEEM and making it quite useful in practical applications.

We also found that the refocused primary (RP) ESEEM has many properties in common with the 2D four-pulse ESEEM method (*9*) introduced recently by Van Doorslaer and Schweiger as a remedy for blind spots appearing in a one-dimensional four-pulse ESEEM experiment (*13*). As we realized, both techniques can be used for solving similar problems, and we believed that it is appropriate to discuss their features in parallel.

EXPERIMENTAL

To demonstrate the application of the RP ESEEM technique, two kinds of samples have been used. One of them was a

[1] On leave from the Institute of Chemical Kinetics and Combustion, 630090 Novosibirsk, Russia.

[2] To whom correspondence should be addressed. Fax: (520) 621-8407. E-mail: andrei@u.arizona.edu.

1090-7807/00 $35.00

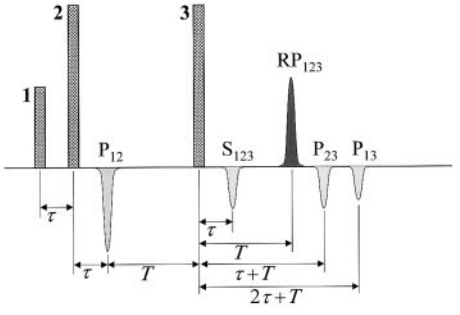

FIG. 1. Pulse sequence of the refocused primary ESEEM method. The mw pulses are denoted by the numbers "1," "2," and "3." The primary ESE signals are denoted as "P_{ij}," with i and j standing for the numbers of the mw pulses responsible for their formation. The stimulated ESE signal formed by all three pulses is denoted "S_{123}." The refocused primary ESE signal is denoted "RP_{123}." Time intervals between the mw pulses and various ESE signals are shown.

glassy toluene solution of 2,2,6,6-tetramethyl-1-piperidinyloxy (TEMPO) stable free radical obtained from Aldrich. The other sample contained a Mo(V) center in the high-pH (pH 9.5) form of sulfite oxidase extracted from chicken liver and prepared as described elsewhere (*14*).

The experiments have been performed on a homebuilt broadband pulsed EPR spectrometer (*15*) operating in the range of microwave (mw) frequencies from 2 to 8 GHz. The durations of all mw pulses were 20 ns. The measurement temperature was about 20 K.

THEORY

1. Pulse sequence. The pulse sequence for detection of the RP ESE signal consists of three mw pulses (see Fig. 1). The first two pulses separated by time interval τ generate the primary ESE signal, P_{12}. The third mw pulse is applied at time interval T after the primary ESE signal to refocus it into RP_{123} that appears at time interval T after the third pulse. The unwanted primary (P_{13}, P_{23}) and stimulated (S_{123}) echoes are eliminated by a phase cycling procedure outlined below. The refocused signal can be detected at any τ if T exceeds the intrinsic spectrometer dead time t_d, thus providing virtually zero dead time along the τ coordinate. Since two time variables are involved, the RP ESEEM represents a 2D spectroscopy that can provide useful correlations of nuclear transitions. In the following section we consider these correlations theoretically in some detail.

2. Theoretical analysis. To explicitly present the features of the RP ESE avoiding exceedingly complicated expressions, let us consider the simplest spin system consisting of interacting electron and nuclear spins (S and I, respectively) of $\frac{1}{2}$. The spin Hamiltonian of this system in a laboratory coordinate frame (XYZ) with axis **Z** being parallel to the direction of the static magnetic field $\mathbf{B}_0$ is

$$\hat{H} = g_e\beta_e B_0\hat{S}_Z - \nu_I\hat{I}_Z + (a_{iso} + T_{ZZ})\hat{S}_Z\hat{I}_Z + T_{ZX}\hat{S}_Z\hat{I}_X + T_{ZY}\hat{S}_Z\hat{I}_Y, \quad [1]$$

where g_e is the electronic g factor, β_e is the Bohr magneton, $\nu_I = g_n\beta_n B_0$ is a nuclear Zeeman frequency (g_n is the nuclear g factor and β_n is the nuclear magneton), a_{iso} is an isotropic hfi constant, and T_{ij} are the components of the anisotropic hfi tensor.

Applying a density matrix formalism (*16*), after the usual procedure of selecting the desired spin echo signal, we readily obtain the expression for the RP ESE,

$$V(\tau, T, t|\Delta\omega) \propto \mathrm{Im}[\alpha_1\beta_1\beta_2^{*2}\beta_3^2\exp(-i\Delta\omega t) \times \mathrm{Tr}\{\mathbf{B}^+_{t+T}\mathbf{M}^+\mathbf{A}^+_{t+T}\mathbf{M}\mathbf{B}^+_{\tau}\mathbf{M}^+\mathbf{A}^+_{\tau}\mathbf{M}\mathbf{B}^+_{t+\tau}\mathbf{M}^+\mathbf{A}^+_{t+\tau}\mathbf{M}\}] \quad [2]$$

$$\alpha_k = \cos\left(\frac{\omega_{Nk}t_{pk}}{2}\right) - i\cos\phi_k\sin\left(\frac{\omega_{Nk}t_{pk}}{2}\right);$$

$$\beta_k = -i\sin\phi_k\sin\left(\frac{\omega_{Nk}t_{pk}}{2}\right)$$

$$\tan\phi_k = \omega_{1k}/\Delta\omega; \quad \omega_{Nk} = \sqrt{\omega_{1k}^2 + \Delta\omega^2}$$

$$\mathbf{M} = \begin{pmatrix} \sqrt{\frac{1+\sqrt{1-k}}{2}} & \sqrt{\frac{1-\sqrt{1-k}}{2}} \\ -\sqrt{\frac{1-\sqrt{1-k}}{2}} & \sqrt{\frac{1+\sqrt{1-k}}{2}} \end{pmatrix};$$

$$\mathbf{A}_\xi = \begin{pmatrix} \exp\left(i\frac{\omega_\alpha\xi}{2}\right) & 0 \\ 0 & \exp\left(-i\frac{\omega_\alpha\xi}{2}\right) \end{pmatrix}$$

$$\mathbf{B}_\xi = \begin{pmatrix} \exp\left(i\frac{\omega_\beta\xi}{2}\right) & 0 \\ 0 & \exp\left(-i\frac{\omega_\beta\xi}{2}\right) \end{pmatrix},$$

where ω_{1k} is the amplitude of the kth pulse in angular frequency units, $\Delta\omega$ is a frequency offset from resonance, and t is a spin echo coordinate ($t = 0$ corresponds to the time interval T after the third pulse). The nuclear transition frequencies $\omega_\alpha = 2\pi\nu_\alpha$ and $\omega_\beta = 2\pi\nu_\beta$ at α and β electron spin manifolds, respectively, are given by

$$\nu_\alpha = \sqrt{\frac{T_{ZX}^2 + T_{ZY}^2}{4} + \left(\nu_I - \frac{a_{iso} + T_{ZZ}}{2}\right)^2};$$

$$\nu_\beta = \sqrt{\frac{T_{ZX}^2 + T_{ZY}^2}{4} + \left(\nu_I + \frac{a_{iso} + T_{ZZ}}{2}\right)^2}. \quad [3]$$

The modulation amplitude factor k is

$$k = \nu_I^2(T_{ZX}^2 + T_{ZY}^2)/(\nu_\alpha\nu_\beta)^2. \quad [4]$$

Equation [2] is factorized into a product of two terms. The term outside the trace sign gives the shape of the ESE signal as determined by the mw pulse parameters and reproduces the expression derived in Ref. (*17*). The term under the trace sign describes the ESEEM. Though Eq. [2] already represents an analytical solution for the RP ESEEM and may be used in numerical simulations, a more convenient expression can be derived after calculation of Im[. . .] at $t = 0$,

$$V(\tau, T) \propto 1 - \frac{k}{4}\left\{3 - c_\alpha - c_\beta - c_{\alpha'} - c_{\beta'} - c_{\alpha+\alpha'} - c_{\beta+\beta'} + \frac{1+\sqrt{1-k}}{2}(c_\delta + c_{\delta'} - c_{\alpha+\beta'} - c_{\beta+\alpha'} + c_{\alpha+\sigma'} + c_{\sigma+\alpha'} + c_{\beta+\sigma'} + c_{\sigma+\beta'} - c_{\sigma+\sigma'}) + \frac{1-\sqrt{1-k}}{2} \times (c_\sigma + c_{\sigma'} - c_{\alpha-\beta'} - c_{\beta-\alpha'} + c_{\alpha+\delta'} + c_{\delta+\alpha'} + c_{\beta-\delta'} + c_{\delta-\beta'} - c_{\delta+\delta'})\right\}, \quad [5]$$

where, due to a large number of harmonics, a brief notation is used with the characters "c" standing for cosine functions. The subscripts α, β, σ, δ, α', β', σ', and δ' denote the arguments of the cosines $2\pi\nu_\alpha\tau$, $2\pi\nu_\beta\tau$, $2\pi\nu_\sigma\tau$, $2\pi\nu_\delta\tau$, $2\pi\nu_\alpha T$, $2\pi\nu_\beta T$, $2\pi\nu_\sigma T$, and $2\pi\nu_\delta T$, respectively. $\nu_\sigma = \nu_\alpha + \nu_\beta$ and $\nu_\delta = \nu_\alpha - \nu_\beta$ are the sum and difference combination frequencies.

Equation [5] describes the oscillations of the RP ESE signal with nuclear fundamental frequencies, ν_α and ν_β, and their linear combinations, ν_σ and ν_δ, in both τ and T dimensions. One can see that while some terms in Eq. [5] depend only on τ or T, the others depend on both time intervals and describe the phase correlations between the oscillations in τ and T dimensions. Equation [5] is symmetric with respect to τ and T. If one of these time intervals equals zero, Eq. [5] reduces to the usual expression for the two-pulse ESEEM. For example, for $T = 0$,

$$V(\tau) = 1 - (k/2)[1 - c_\alpha - c_\beta + \tfrac{1}{2}(c_\delta + c_\sigma)]. \quad [6]$$

The expression for the ESEEM in the 2D four-pulse technique (*9*) (the pulse sequence $\pi/2$–τ–$\pi/2$–T–π–T–$\pi/2$–τ–echo), which, following the authors of Ref. (*9*), is referred to as "2D-CP" ("CP" stands for "combination peak") and discussed in this section in parallel with the RP ESEEM, may be written as

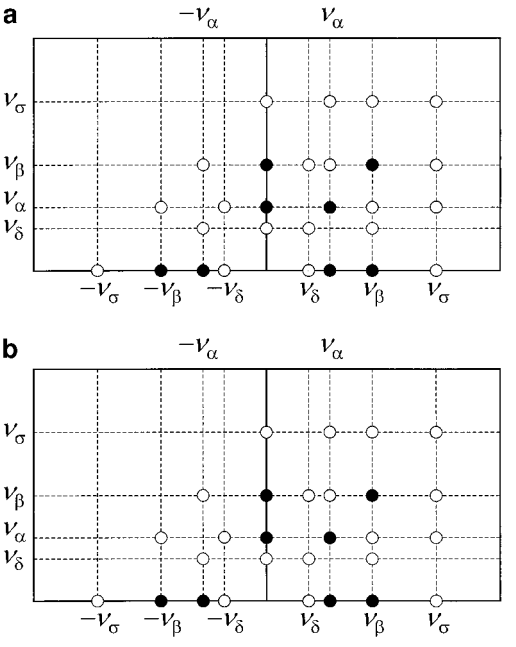

FIG. 2. The positions and intensities of various lines in the 2D spectra of RP ESEEM (a) and 2D-CP ESEEM (b). The diagrams correspond to a weakly coupled ($|a_{iso} + T_{ZZ}| < 2\nu_I$) nucleus with $I = \frac{1}{2}$ in an oriented system (with unspecified orientation). Black circles denote the lines with intensities proportional to k. Gray circles denote the lines with intensities proportional to $k(1 + \sqrt{1-k})$. White circles show the lines with intensities proportional to $k(1 - \sqrt{1-k})$. The horizontal axis corresponds to the FT along τ. The vertical axis corresponds to the FT along T.

$$V(\tau, T) \propto 1 - \frac{k}{4}\left\{3 - c_\alpha - c_\beta - c_{\alpha'} - c_{\beta'} - c_{\alpha+\alpha'} - c_{\beta+\beta'} + \frac{1+\sqrt{1-k}}{2}(-c_\delta + c_{\sigma'} + c_{\alpha+\beta'} + c_{\beta+\alpha'} - c_{\alpha+\sigma'} + c_{\delta+\alpha'} - c_{\beta+\sigma'} + c_{\delta-\beta'} + c_{\sigma+\sigma'}) + \frac{1-\sqrt{1-k}}{2} \times (-c_\sigma + c_{\delta'} + c_{\alpha-\beta'} + c_{\beta-\alpha'} - c_{\alpha+\delta'} + c_{\sigma+\alpha'} - c_{\beta-\delta'} + c_{\sigma+\beta'} + c_{\delta+\delta'})\right\}, \quad [7]$$

where the primed arguments correspond to the time interval T.

One has to note that Eqs. [5] and [7] and Eqs. [8] and [9] (see below) are valid for the case of weak hfi ($|a_{iso} + T_{ZZ}| < 2\nu_I$). In the case of strong hfi ($|a_{iso} + T_{ZZ}| > 2\nu_I$) the factors $(1 + \sqrt{1-k})/2$ and $(1 - \sqrt{1-k})/2$ should be interchanged.

A natural way to perform the RP and 2D-CP ESEEM experiments is to acquire a 2D data set, τ vs T. The Fourier transformation (FT) of the 2D time-domain data will produce a 2D spectrum with the positions of various lines evident from Eqs. [5] and [7]. As an example, Figs. 2 and 3 show the

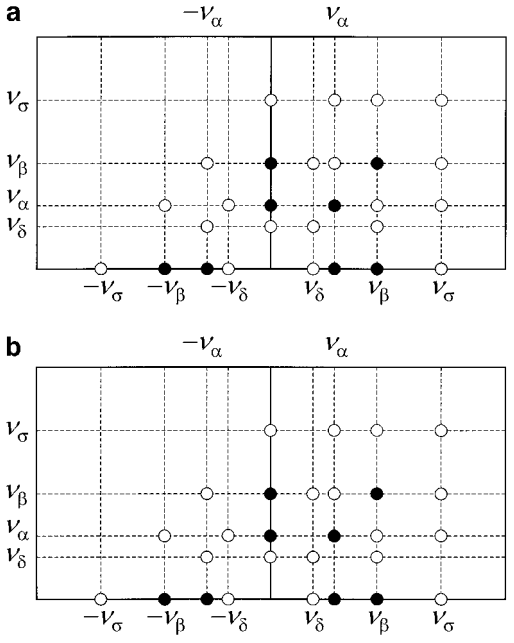

FIG. 3. The positions and intensities of various lines in the 2D spectra of RP ESEEM (a) and 2D-CP ESEEM (b). The diagrams correspond to a strongly coupled ($|a_{\rm iso} + T_{ZZ}| > 2\nu_{\rm I}$) nucleus with $I = \frac{1}{2}$ in an oriented system (with unspecified orientation). Notations are the same as those in Fig. 2.

intensities of various lines in RP and 2D-CP ESEEM spectra of an oriented system with a single nucleus, expected in situations of weak and strong hfi, respectively. One can see from Eqs. [5] and [7] and Figs. 2 and 3 that, apart from the permutation of harmonics, the 2D spectra of RP and 2D-CP ESEEM are similar and differ only in intensities of various lines.

Before considering the simulated and experimental 2D spectra, we have to describe notations and data processing used in this work. The horizontal (ν) and vertical (ν') frequency axes in the 2D spectra correspond to the FTs along τ and T, respectively. The 2D spectra were obtained in two steps, by performing separate FTs for each time manifold. Before each FT, the nonoscillating background was subtracted from the time-domain data in the corresponding time manifold. This processing resulted in a suppression of the spectrum lines situated along ν at $\nu' = 0$ and along ν' at $\nu = 0$, but retained the features correlating different harmonics we were mostly interested in. The frequency positions of the 2D spectrum lines are given in the (ν, ν') format. The correlation assignments are given in parentheses, with the symbols α, β, σ, and δ standing for ν_α, ν_β, ν_σ, and ν_δ, respectively.

Let us now briefly discuss the spectra in a disordered system. Figures 4a and 4b show the (++) quadrants of the spectra of RP and 2D-CP ESEEMs, respectively, calculated for one weakly coupled proton with $\nu_{\rm I} = 8$ MHz, $a_{\rm iso} = 0$ MHz, and $T_\perp = -3$ MHz (where $T_\perp$ is the perpendicular component of the axial anisotropic hfi tensor). The (−+) quadrants are not shown because most of the lines contributing there are very weak due to the amplitude factor proportional to $1 - \sqrt{1-k}$. The only line that has an amplitude proportional to $1 + \sqrt{1-k}$ is the (δ, α) line in 2D-CP spectrum (see Fig. 2b). However, the amplitude of this line is small because of its large width of $3|T_\perp|$ in the ν manifold (twice that of the (α, β) and (β, α) correlation lines). Besides, because of a very low frequency in the ν manifold, this line is suppressed as a result of the time-domain background subtraction.

The structure of spectra in the (++) quadrants is easily understood from comparison with Fig. 2. The intersecting diagonal ridges centered at a frequency of about (8.3, 8.3) MHz are the (α, β) and (β, α) correlations. The narrow peak located on the main diagonal at about (16.6, 16.6) MHz is the (σ, σ) correlation. The pair of ridges situated at $\nu' \approx 16.6$ MHz and extending almost parallel to the ν axis are the (α, σ) and (β, σ) correlations. These lines are similar in both types of spectra. In addition, the RP ESEEM spectrum shows a pair of ridges at $\nu = 16.6$ MHz oriented approximately parallel to the ν' axis. These are the (σ, α) and (σ, β) correlation lines.

It is important to note that RP ESEEM exhibits virtually zero dead time along the τ coordinate, whereas in the 2D-CP method the zero dead time axis is T. Thus, in the RP ESEEM spectra the dead time will have a greater influence on the lines extended along the ν' axis, while in the 2D-CP method the lines extended along the ν axis will suffer the most. As an example, Figs. 4c and 4d show the spectra of RP and 2D-CP ESEEM, respectively, calculated with the dead time $t_{\rm d} = 200$

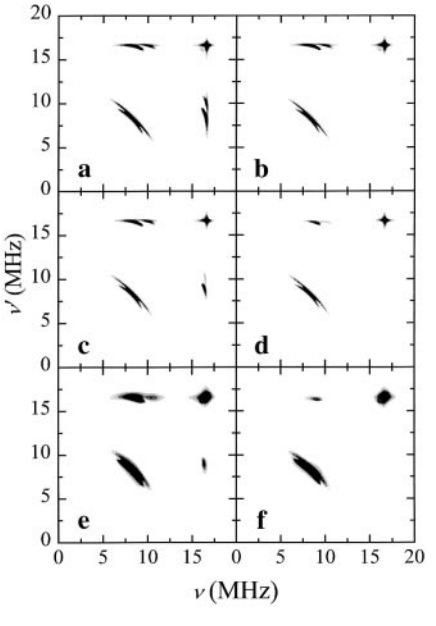

FIG. 4. The calculated 2D spectra of RP ESEEM (a, c, e) and 2D-CP ESEEM (b, d, f) in an orientationally disordered system. The calculation is performed for a weakly coupled nucleus with $I = \frac{1}{2}$, $\nu_{\rm I} = 8$ MHz, $a_{\rm iso} = 0$ MHz, and $T_\perp = -3$ MHz. In panels (a) and (b) the dead time $t_{\rm d}$ equals zero. In panels (c) and (d) $t_{\rm d} = 200$ ns along time axes T and τ, respectively. Panels (e) and (f) are the same as the respective panels (c) and (d), but with the $T_\perp$ value being Gaussian-distributed around −3 MHz, with the distribution width of 1 MHz between the maximum slope points.

ns (a typical value for our S/C band experiments) along the appropriate axes as discussed above. One can see that the intensity of the (α, σ) and (β, σ) lines in the 2D-CP spectra has decreased considerably relative to the original one and to that in the RP ESEEM spectrum (c). The situation here is saved to some extent by the fact that the harmonics corresponding to spectrum singularities exhibit long decay times and survive even after considerable dead time (*1*).

In many actual systems, however, the spectrum singularities can be much less pronounced because of the distribution of hyperfine interactions associated with some structural disorder. This will result in a greater suppression of the (α, σ) and (β, σ) correlation lines in 2D-CP spectra and may easily render them unobservable. This is illustrated in Figs. 4e and 4f representing the spectra of RP and 2D-CP ESEEM, respectively, calculated with $t_d = 200$ ns and with hfi parameters similar to those used above. The only difference consisted in introducing a Gaussian distribution of $T_\perp$ around the central value of -3 MHz with the width between the maximum slope points of 1 MHz. One can see that the (α, σ) and (β, σ) correlation lines in Fig. 4f are barely discernible (same as the (σ, α) and (σ, β) lines in Fig. 4e), while in Fig. 4e they are clearly visible.

The dead time of 200 ns used in the calculations presented in Figs. 4c–4f is typical for our ESEEM experiments at low mw frequencies (S and C bands). At higher mw frequencies considerably shorter (two to three times in the X band) instrumental dead time can be achieved for the same quality factor of the resonator. Therefore, the influence of the dead time on the appearance of the 2D spectra of RP and 2D-CP ESEEM at high-frequency bands will be generally less noticeable.

The RP and 2D-CP ESEEM spectra simulated for a strongly coupled nucleus with $\nu_I = 1.5$ MHz, $a_{iso} = 12$ MHz, and $T_\perp = -1$ MHz (with these parameters it could be ^{15}N ligand to the paramagnetic metal ion as observed in the X band) in a disordered system are shown in Fig. 5. The most intense lines in these spectra correspond to (α, β) and (β, α) correlations (diagonal ridges in the ($-+$) quadrant), (α, σ) and (σ, α) correlations (horizontal and vertical ridges in the ($-+$) quadrant), (β, σ) and (σ, β) correlations (horizontal and vertical ridges in the ($++$) quadrant), and the (σ, σ) correlation (narrow peak on the main diagonal of the ($++$) quadrant). Due to the self-suppression effect (see the Appendix), the (α, α) and (β, β) correlation lines situated on the main diagonal of the ($++$) quadrant in Figs. 4 and 5 are barely discernible in spite of the fact that their amplitude is proportional to k (see Eqs. [5] and [7] and Figs. 2 and 3).

In the 2D spectra shown in Figs. 4 and 5 the lines situated along ν at $\nu' = 0$ and along ν' at $\nu = 0$ were suppressed by the time-domain background subtraction in order to avoid distracting the attention from the correlation lines. Now we will consider the spectra at $\nu = 0$ and at $\nu' = 0$ as usual 1D spectra along ν' and ν, respectively. Clearly, it is most interesting to consider the spectra corresponding to the zero dead time manifold.

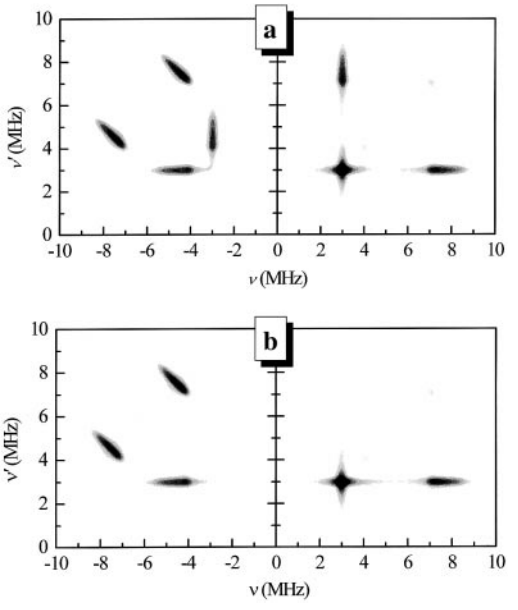

FIG. 5. The calculated 2D spectra of RP ESEEM (a) and 2D-CP ESEEM (b) in an orientationally disordered system. The calculation is performed for a strongly coupled nucleus with $I = \frac{1}{2}$, $\nu_I = 1.5$ MHz, $a_{iso} = 12$ MHz, and $T_\perp = -1$ MHz. The dead time t_d equals zero. The left and right panels represent the ($-+$) and ($++$) quadrants, respectively.

In RP ESEEM the zero dead time manifold is τ, and the 1D spectrum we will discuss corresponds to the slice of the 2D spectrum situated at $\nu' = 0$. This slice is obtained by integration of Eq. [5] over T. To a good approximation (at least, when the periods of all harmonics are shorter than the integration interval), the integration will result in the averaging of all harmonics containing T to zero. Equation [5] in this case reduces to

$$V(\tau) = 1 - \frac{k}{4}\left[3 - c_\alpha - c_\beta + \frac{1+\sqrt{1-k}}{2}\,c_\delta + \frac{1-\sqrt{1-k}}{2}\,c_\sigma\right] \qquad [8]$$

which resembles the usual expression for the primary ESEEM (Eq. [6]), but contains the ν_σ and ν_δ harmonics scaled with the additional factors depending on k. For $k \to 0$ the contribution of ν_σ to Eq. [8] becomes small. This feature is extremely useful for suppressing the ν_σ lines of distant protons ($k \ll 1$) and revealing the ν_σ lines of close protons that may be poorly resolved in the usual primary ESEEM spectrum. For the latter protons the modulation amplitude factor $k \sim 1$ may be easily achieved by selecting the resonance conditions (the operational mw frequency and magnetic field B_0) as to mutually compensate nuclear Zeeman and hyperfine interactions.

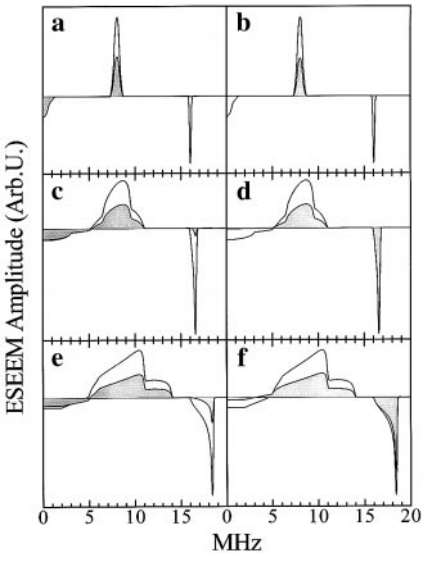

FIG. 6. Calculated spectra of primary ESEEM, RP ESEEM integrated over T, and 2D-CP ESEEM integrated over τ for a proton with $\nu_I = 8$ MHz and $a_{iso} = 0$ MHz in a disordered system. The anisotropic hfi values $T_\perp$ are -0.632 MHz (a, b), -3 MHz (c, d), and -6 MHz (e, f). The dead time is equal to zero. Shaded traces, the spectra of the integrated RP ESEEM (a, c, e) and integrated 2D-CP ESEEM (b, d, f). Traces without filling, the spectra of primary ESEEM. As $T_\perp = -0.63$ MHz corresponds to the electron–proton distance of about 5 Å, panel (a) models the RP ESEEM of distant matrix protons and demonstrates a practically complete suppression of the ν_σ harmonic in this situation.

In the 2D-CP technique the zero dead time coordinate is T. Integrating Eq. [7] over τ we obtain the ESEEM that will correspond to the slice of the 2D spectrum at $\nu = 0$:

$$V(T) = 1 - \frac{k}{4}\left[3 - c_{\alpha'} - c_{\beta'} + \frac{1-\sqrt{1-k}}{2}\,c_{\delta'} + \frac{1+\sqrt{1-k}}{2}\,c_{\sigma'}\right]. \qquad [9]$$

As follows from Eq. [9], the integrated 2D-CP ESEEM practically does not change the amplitudes of the ν_σ harmonics of distant protons but efficiently suppresses their ν_δ harmonics. All these features are demonstrated in Fig. 6, where integrated spectra of the RP and 2D-CP ESEEM are compared with conventional two-pulse ESEEM at various magnitudes of hyperfine interactions.

Figure 7 gives an example of the spectra obtained from the integrated RP and 2D-CP ESEEM in the case of a disordered system consisting of a pool of distant matrix protons (approximated by 30 protons at a distance of 5 Å from the unpaired electron) and a single close proton with $a_{iso} = 0$ MHz and $T_\perp = -3$ MHz. The proton Zeeman frequency in these calculations was 8 MHz. Trace 1 in Fig. 7 is a cosine FT spectrum of usual primary ESEEM calculated with zero dead time. Shaded trace 2 in the same figure is a spectrum of the integrated RP ESEEM. The total time interval used for the FT was 2 μs in both cases, which approximates the transverse relaxation time T_2 typical for organic radicals and many low-spin metal-centered paramagnetic sites at cryogenic temperatures. One can see that in the primary ESEEM spectrum the shifted ν_σ line due to the close proton manifests itself as a shoulder at the high-frequency side of the much more intense ν_σ line of the distant protons situated at $2\nu_I = 16$ MHz. In the spectrum of the integrated RP ESEEM, however, the situation is opposite. The matrix ν_σ line is considerably suppressed and that due to the close proton is clearly visible.

Trace 3 in Fig. 7 is a cosine FT spectrum of the integrated 2D-CP ESEEM. The total time interval used for the FT (generally determined by the longitudinal relaxation time T_1) was 5 μs. This spectrum shows that the increase in the time-domain record length also allows one to separate the ν_σ lines due to the close and distant protons and represents an example of a usual resolution-enhancement approach.

The position of the ν_σ line in the spectra can be used to determine the anisotropic hfi of the nuclei in the vicinity of the unpaired electron (see Eq. [13] below). Figure 7 demonstrates that both RP and 2D-CP ESEEM methods allow one to separate the ν_σ line due to close nuclei from that arising due to distant matrix protons. In the first case this separation is based on the amplitude suppression of the matrix ν_σ line. In the second case it is achieved by extending the registration interval T and compressing the matrix ν_σ line in the frequency domain.

In previous examples (see Fig. 6) we have varied $T_\perp$ in order to change the ESEEM amplitude factor k. Another way to

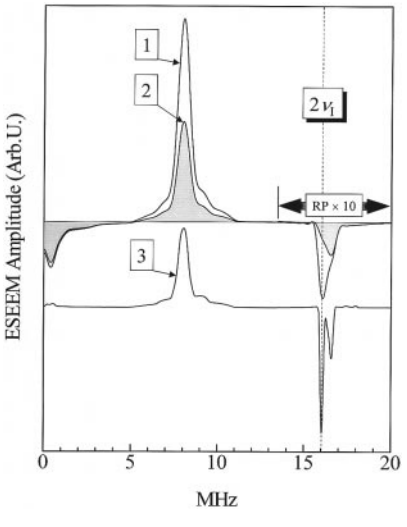

FIG. 7. Calculated spectra of primary ESEEM (trace 1), RP ESEEM integrated over T (shaded trace 2), and 2D-CP ESEEM integrated over τ (trace 3) for 30 protons with $a_{iso} = 0$ MHz and $T_\perp = -0.632$ MHz (corresponds to a distance of 5 Å) and 1 proton with $a_{iso} = 0$ MHz and $T_\perp = -3$ MHz in a disordered system. The proton Zeeman frequency is $\nu_I = 8$ MHz. The total time-domain data length was 2 μs for traces 1 and 2, and 5 μs for trace 3. The dashed line shows the position of the double Zeeman frequency of protons.

change k is by adjusting the mw carrier frequency accompanied by a proportional change of the resonant magnetic field B_0. In this way one can always achieve a condition when, at least, for part of the orientations of a paramagnetic center, the hyperfine interaction of close protons at one of the electron spin manifolds is compensated by their Zeeman interaction (e.g., for purely anisotropic hfi it can be expressed as $|\nu_I| \leq |T_\perp|$), resulting in a resonance-like increase of the amplitude factor k (see Eq. [4]). At the same time, the distant matrix protons will still be far from the cancellation condition and their amplitude factor k will be small. Thus, the variation of the operational frequency of the pulsed EPR spectrometer provides a means for controlling the relative intensities of the sum combination lines due to close and distant nuclei in the RP ESEEM technique. Of course, the increase of the relative intensity of the ESEEM due to close protons at Zeeman/hfi cancellation will take place in all ESEEM techniques, but for the ν_σ lines in RP ESEEM it is much more pronounced due to the nonlinear dependence of their amplitudes on k.

To complete the comparison of the RP and 2D-CP ESEEM, let us consider the intensities of the ESE signals in these techniques. For simplicity, we will assume the nominal flip angles in RP ESE to be 90°, 180°, and 180° and the pulses in 2D-CP ESE to be 90°, 90°, 180°, and 90°. All the 90° pulses will be assumed to have the same amplitude ω_1 and duration t_p. The 180° pulses also will have the same amplitude $\tilde{\omega}_1$ and duration $\tilde{t}_p$. The general expressions for the ESE amplitudes in the RP (V_{RP}) and 2D-CP (V_{4p}) methods then can be written as

$$V_{RP} = \frac{\omega_1}{\omega_N}\frac{\tilde{\omega}_1^4}{\tilde{\omega}_N^4}\sin(\omega_N t_p)\sin^4\left(\frac{\tilde{\omega}_N\tilde{t}_p}{2}\right)$$

$$V_{4p} = \frac{\omega_1^3}{2\omega_N^3}\frac{\tilde{\omega}_1^2}{\tilde{\omega}_N^2}\sin^3(\omega_N t_p)\sin^2\left(\frac{\tilde{\omega}_N\tilde{t}_p}{2}\right), \qquad [10]$$

where $\omega_N = \sqrt{\omega_1^2 + \Delta\omega^2}$ and $\tilde{\omega}_N = \sqrt{\tilde{\omega}_1^2 + \Delta\omega^2}$ are the nutation frequencies during the 90° and 180° pulses, respectively. The expression for V_{RP} directly follows from Eq. [2] and that for V_{4p} is obtained in a similar way using the density matrix formalism. If all the mw pulses have the same amplitude ($\tilde{\omega}_1 = \omega_1$, $\tilde{t}_p = 2t_p$), then

$$V_{RP} = 2V_{4p} = \frac{\omega_1^5}{\omega_N^5}\sin^5(\omega_N t_p). \qquad [11]$$

The amplitude of the RP ESE signal in this case is two times greater than that of the 2D-CP ESE signal.

In practice for HYSCORE and four-pulse ESEEM experiments it is customary to use the 180° pulse with the amplitude as high as possible to maximize the magnetization inversion by the third pulse. For simplicity, we will now consider the limiting situation of ideal (infinitely short) 180° pulses. Equations [10] then reduce to

TABLE 1
Phase Cycle for Eliminating Unwanted Echoes (P_{13}, P_{23}, and S_{123} in Fig. 1) in the RP ESEEM Experiment

First pulse phase	Second pulse phase	Third pulse phase	Operation
0°	0°	0°	+
0°	180°	0°	+
0°	90°	0°	−
0°	270°	0°	−

$$V_{RP} = \frac{\omega_1}{\omega_N}\sin(\omega_N t_p); \quad V_{4p} = \frac{\omega_1^3}{2\omega_N^3}\sin^3(\omega_N t_p). \qquad [12]$$

To obtain the spin echo intensities one has to integrate Eqs. [12] over $\Delta\omega$ with a statistical weight as given by the EPR lineshape $G(\Delta\omega)$. For a usual (when dealing with solid disordered samples) situation of a broad EPR spectrum we can approximate $G(\Delta\omega)$ by a constant. The integration then results in $V_{RP}/V_{4p} \approx 2.28$. For nonideal 180° pulses the ratio V_{RP}/V_{4p} will be between these two limiting values, 2 (obtained from Eq. [11]) and 2.28.

Finally, all unwanted echoes in the RP ESE method (see Fig. 1) are eliminated by the four-step phase cycle shown in Table 1, and the intensity of modulation relative to the nonoscillating term can be obtained in the same simple manner as in a primary echo. The situation is different in the 2D-CP ESE, where the detected signal is a sum of the inverted stimulated echo (the carrier of the four-pulse ESEEM) and the usual stimulated echo arising from nonresonant spins that are not inverted by the third pulse. These two signals cannot be separated by phase cycling. As a result, the determination of the intensity of the four-pulse ESEEM relative to the nonoscillating term *of the four-pulse echo* in the 2D-CP technique becomes quite complicated (*18*) and inaccurate. Therefore, for all practical purposes, a very important advantage of the ESEEM spectroscopy, namely, the possibility to determine the number of nuclei interacting with the unpaired electron, is lost with 2D-CP. Also, it seems appropriate to note here that though the remote-detection implementation of HYSCORE (*8*) (a method closely related to 2D-CP) exhibits zero dead time and lacks the blind spots, it suffers from the same problem as the 2D-CP method and, in practice, does not allow one to accurately determine the number of nuclei contributing to the ESEEM.

A disadvantage of the RP ESE method as compared with 2D-CP is its low frequency resolution limited by the transverse relaxation along both time coordinates. In 2D-CP, the decay of the ESE signal along the T coordinate is governed by the much slower longitudinal relaxation, thus providing a high resolution in the ν' manifold. Therefore, if a high spectral resolution is not required, the RP ESEEM application seems to be preferable because it facilitates a direct comparison between calculated and experimental modulation amplitudes, thus giving the pos-

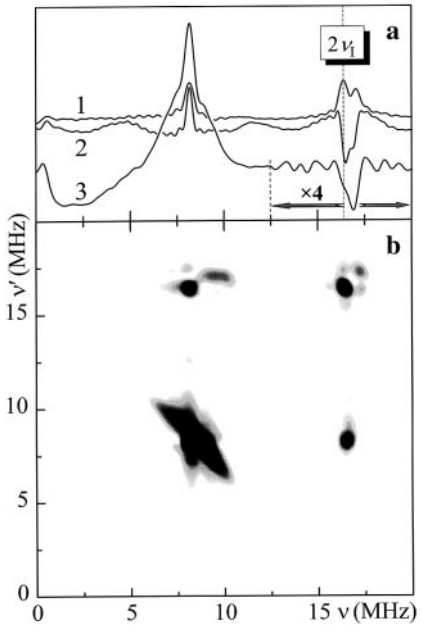

FIG. 8. ESEEM spectra of the stable nitroxide radical TEMPO in toluene obtained at $\nu_{mw} = 5.405$ GHz and $B_0 = 193$ mT. (a) Traces 1 and 2, the magnitude and cosine FT spectra of the primary ESEEM, respectively. Trace 3, the spectrum of the RP ESEEM integrated over T. The relative scaling of the primary and RP ESEEM spectra is arbitrary. (b) 2D spectrum of the RP ESEEM.

sibility of determining the number of nuclei contributing to the ESEEM. On the other hand, if spectral resolution is important, the 2D-CP method may be preferable, especially if the number of nuclei contributing to the ESEEM is known *a priori.* One can also use both methods in a complementary fashion, employing 2D-CP to obtain a highly resolved spectrum and estimate the hfi parameters, and RP ESEEM to estimate the number of nuclei.

EXPERIMENTAL RESULTS

The experimental results presented here are only aimed to demonstrate the key features of the 2D implementation of the RP ESEEM technique. Therefore, in the examples below we will refrain from detailed spectroscopic analysis, stressing only the observability of the spectral features due to close protons and giving simple estimates of the coupling values.

1. Radical TEMPO in glassy toluene solution. Figure 8b shows a 2D spectrum of the RP ESEEM for the frozen glassy solution of the nitroxide radical TEMPO in toluene. To provide better resolution of the ν_σ spectral region, this experiment was performed at a relatively low mw carrier frequency of 5.405 GHz and at the magnetic field $B_0 = 193$ mT corresponding to the maximum of the field-sweep ESE spectrum (not shown). The spectrum in Fig. 8b is similar to the simulated spectrum in Fig. 4e. The only qualitative difference between them is that the experimental spectrum in Fig. 8b is contributed not only by close protons of the methyl groups but also by the pool of more weakly coupled protons from solvent and the radical itself. The latter protons give rise to four peaks located at (8.2, 8.2) MHz (8.2 MHz is the Zeeman frequency of protons at $B_0 = 193$ mT) corresponding to the (α, β) and (β, α) correlations, at (8.2, 16.4) MHz corresponding to the (α, σ) and (β, σ) correlations, at (16.4, 8.2) MHz corresponding to the (σ, α) and (σ, β) correlations, and at (16.4, 16.4) MHz corresponding to the (σ, σ) correlation.

The ridges oriented perpendicular to the main diagonal in the vicinity of (ν_I, ν_I) are the (α, β) and (β, α) correlation lines of the close methyl protons. In addition, these protons give rise to a ridge at $\nu' \approx 17.05$ MHz extending along ν from about 8 MHz up to about 10.5 MHz. This ridge is similar to that in Fig. 4e and corresponds to the (α, σ) and (β, σ) correlations. Same as in Fig. 4e, the lines (σ, α) and (σ, β) are suppressed by the dead time ($t_d \approx 300$ ns) along the T coordinate. Finally, the peak at (17.2, 17.2) MHz is a (σ, σ) correlation line of the methyl protons. It has been shown (*19*) that in a disordered system

$$\nu_\sigma \approx 2\nu_I + T_\perp^2/2\nu_I. \qquad [13]$$

Thus, from $\nu_\sigma \approx 17.2$ MHz the anisotropic hfi value $T_\perp \approx -3.6$ MHz can be estimated (the negative sign is chosen from physical considerations).

Figure 8a shows the modulus and cosine FT spectra of the usual primary ESEEM (traces 1 and 2, respectively). Trace 3 is the cosine FT of the integrated (over T) RP ESEEM. One can see that while the primary ESEEM spectra, due to the long dead time ($t_d \approx 200$ ns), do not show any broad lines, the spectrum of the integrated RP ESEEM shows clearly not only the fundamental lines of the methyl protons, but also the difference combination line situated at the frequencies below 5 MHz. As predicted by our theoretical analysis, the sum combination line due to the distant matrix protons in the spectrum of the integrated RP ESEEM is considerably suppressed as compared with the spectrum of the primary ESEEM. The broad peak with positive amplitude situated symmetrically with respect to the proton Zeeman frequency is due to the fundamental frequencies of the methyl protons. The half-height width of this peak is about 3.2 MHz and correlates with the $T_\perp$ value estimated above.

Thus, the RP ESEEM spectra of TEMPO demonstrate all the features of this technique discussed above under Theory. The 1D spectra have shown the suppression of the matrix ν_σ line and the drastic reduction of the dead time, making possible the direct observation of the fundamental and difference combination lines of the methyl protons. In 2D spectra the (α, σ) and (β, σ) correlations were observed, showing the potential of the RP ESEEM technique for facilitating the interpretation of the spectra of paramagnetic centers with unknown structure.

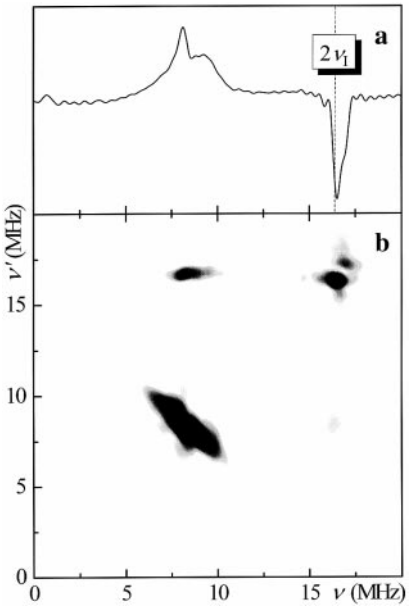

FIG. 9. 2D-CP ESEEM spectra of the stable nitroxide radical TEMPO in toluene obtained at $\nu_{mw} = 5.387$ GHz and $B_0 = 191.8$ mT. (a) The cosine FT spectrum of the 2D-CP ESEEM integrated over τ. (b) 2D spectrum of the 2D-CP ESEEM.

For comparison, Fig. 9b shows the 2D spectrum obtained using the 2D-CP method. This spectrum is similar to that obtained by the RP ESE method (Fig. 8b), but the $(\alpha, \sigma)/(\beta, \sigma)$ correlation region shows only one line slightly shifted from the $2\nu_I$ position in the ν' manifold. This line is obviously contributed by the (α, σ) and (β, σ) lines from both distant matrix and close methyl protons, the latter being somewhat suppressed by the dead time of about 200 ns (see calculations presented in Fig. 4). Besides, the $(\alpha, 2\alpha)$ and $(\beta, 2\beta)$ correlation lines (mainly those due to the distant matrix protons) from the usual stimulated echo (see Ref. (*9*)) contribute to this region. The resulting feature at the $(\nu_I, 2\nu_I)$ position in the 2D spectrum does not allow one to distinguish with certainty the $(\alpha, \sigma)/(\beta, \sigma)$ correlation due to the methyl protons.

Figure 9a shows the spectrum of the integrated (along τ) 2D-CP ESEEM. In agreement with the theoretical results and in contrast to the spectrum of the integrated RP ESEEM (Fig. 8a), the ν_δ line is now completely suppressed and the ν_σ lines due to matrix and close methyl protons have a considerable intensity.

2. Mo(V) center in sulfite oxidase. Recently (*20*) the coordination environment of the Mo(V) center of chicken liver sulfite oxidase in H_2O and D_2O solutions has been investigated. The solutions were buffered at pH 9.5 with ~100 mM Tris-type buffer, which resulted in the so-called high-pH form of the enzyme. In D_2O solution, the ESEEM data definitively indicated the presence of a deuteron close to the Mo(V) center, which was ascribed to an OD (in protonated samples OH) group coordinated to the Mo(V) ion. However, all attempts to directly observe a corresponding nearby proton in H_2O solution were unsuccessful. These attempts included both four- and two-pulse experiments at various operational mw frequencies in the range of 8–16 GHz. It was hypothesized that the nearby proton was not directly observable because it does not occupy a unique position with respect to the Mo(V) center, and thus gives rise to a statistical distribution of hfi parameters. Such a distribution could well result in a substantial decrease in the intensity of the proton lines in the ESEEM spectra.

The range of the operational frequencies ν_{mw} from 8 to 16 GHz used in Ref. (*20*) has been limited by the possibilities of the pulsed EPR spectrometer available at that time. Since it is well known that the largest ESEEM amplitudes are achieved at the cancellation of hyperfine and Zeeman interactions, it was clear that optimal mw frequencies for observing the close proton in sulfite oxidase should be considerably lower, between 3.2 and 6 GHz, as estimated from the parameters determined in the experiments with a D_2O-buffered sample (*20*). It recently became possible for us to perform experiments with sulfite oxidase in this low-frequency range with the construction of a new pulsed EPR spectrometer (*15*). At first, we performed measurements at $\nu_{mw} = 3.6$ GHz, but we did not get enough resolution between fundamental and sum combination lines. Therefore, we repeated the experiments at $\nu_{mw} = 5.404$ GHz ($B_0 = 197$ mT corresponding to the maximum of the Mo(V) field-sweep spectrum in sulfite oxidase) and obtained the spectra presented in Figs. 10 and 11.

Figure 10 shows a 2D spectrum of the RP ESEEM of Mo(V) in sulfite oxidase. The features dominating the 2D spectrum mostly belong to distant matrix protons (the (α, β) and (β, α) lines at about (8.4, 8.4) MHz, the (α, σ) and (β, σ) lines at about (8.4, 16.8) MHz, the (σ, α) and (σ, β) lines at (16.8, 8.4) MHz, and the (σ, σ) line at about (16.8, 16.8) MHz). The expected lines due to the close proton are much more broad, weak, and practically hidden in the background noise. However, the cosine and modulus FT spectra of the integrated RP ESEEM (traces 1 and 3 in Fig. 11, respectively) show very

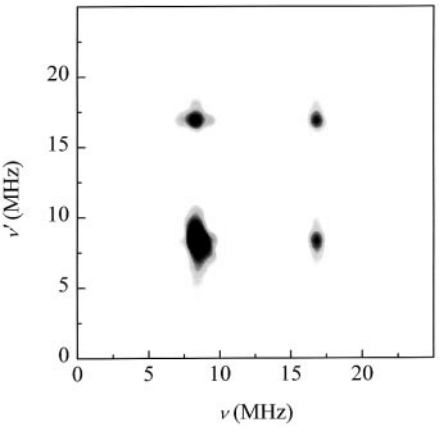

FIG. 10. 2D spectrum of the RP ESEEM of Mo(V) ion in a high-pH form of sulfite oxidase obtained at $\nu_{mw} = 5.404$ GHz and $B_0 = 197$ mT.

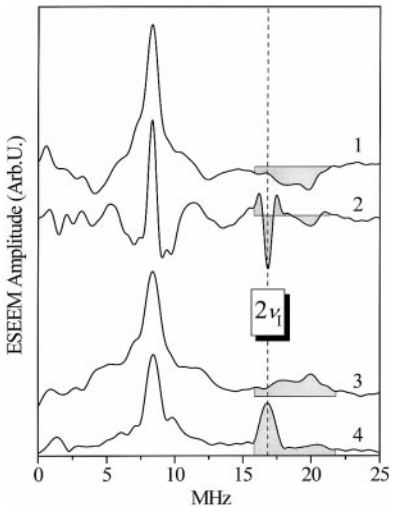

FIG. 11. ESEEM spectra of Mo(V) ion in a high-pH form of sulfite oxidase obtained at $\nu_{mw} = 5.404$ GHz and $B_0 = 197$ mT. Traces 1 and 3, cosine and modulus FT spectra of the RP ESEEM integrated over T, respectively. Traces 2 and 4, cosine and modulus FT spectra of the primary ESEEM. The dashed line shows the position of the double Zeeman frequency of protons.

nicely the presence of the close proton(s). For comparison, the cosine and magnitude spectra of the usual primary ESEEM are shown in Fig. 11 by traces 2 and 4, respectively.

The shaded areas in the spectra in Fig. 11 show the range of the ν_σ lines (including some extra area below the $2\nu_I$ position to account for the finite linewidth). One can see that the matrix ν_σ line (peaking at $2\ \nu_I \approx 16.78$ MHz) clearly visible in the primary ESEEM spectra is almost completely suppressed in the RP ESEEM spectra. On the other hand, the RP ESEEM spectra show a broad ν_σ feature due to the OH proton extending from $2\ \nu_I$ to the higher frequencies of up to 20.5 MHz, with a maximum at about 19.9 MHz. Substituting the position of this maximum into Eq. [13], we can estimate the anisotropic hfi constant $T_\perp \approx -7.2$ MHz. However, the great width of the ν_σ line shows that the anisotropic hfi value is distributed rather than unique. Thus, the estimated $T_\perp$ constant may be considered as being close to the upper limit of possible $T_\perp$ values in this distribution. This estimate agrees with that done in Ref. (*20*) ($T_\perp \approx -1.24$ MHz for the deuteron in the OD group) but is obtained very simply, without performing any numerical simulations.

The fundamental lines of the OH proton are observed as broad features situated in the frequency range from about 4.5 to about 12.5 MHz, symmetrically with respect to $\nu_I \approx 8.39$ MHz, and are in a good correspondence with the estimated anisotropic hfi value. In addition, a pair of poorly resolved shoulders of the fundamental matrix line at frequencies of about 7–7.2 and 9.6–9.8 MHz indicates a contribution of a proton(s) with $T_\perp \approx -(2.6\text{–}2.8)$ MHz. Apart from the OH proton, there is only one possible source of close protons in the Mo center of sulfite oxidase, namely, the β-methylene group of the cysteine residue coordinated to the Mo ion (*21*). The distance of about 3.1 ± 0.1 Å obtained from the above value of $T_\perp$ closely corresponds to the conceivable distance from Mo to the methylene protons of the cysteine residue. Therefore, we will tentatively assign the spectral features mentioned above to the β-methylene protons of the cysteine.

In the magnitude spectrum of the usual primary ESEEM (trace 4 in Fig. 11) all spectral features of the close protons are much less pronounced because of the dead time of about 200 ns. Comparison with trace 3 shows that the fundamental lines due to the close protons observed in trace 4 are mostly those ascribed to the β-methylene group of the cysteine ligand and characterized by relatively weak anisotropic hfi. In the cosine FT spectrum (trace 2 in Fig. 11) the lines due to the close protons are very difficult to trace because of the distortions introduced by the linear phase correction. The ν_δ line clearly visible in the spectrum of the integrated RP ESEEM of the nitroxide radical (trace 3 in Fig. 8a) is not easily observed in Fig. 11. Given the estimated value of anisotropic hfi in sulfite oxidase $T_\perp \approx -7.2$ MHz, this line is expected to occupy the frequency range from zero to about 14 MHz and is mostly hidden under the fundamental lines. The ν_δ lines due to the OH and cysteine protons thus manifest themselves as the negative features surrounding the fundamental lines due to the OH proton in the spectrum of the integrated RP ESEEM (trace 1 in Fig. 11).

A detailed investigation of Mo(V) in sulfite oxidase utilizing RP ESEEM including additional measurements at various positions of the anisotropic EPR spectrum and variation of the operation frequency, simulations of the ESEEM spectra, and the verification of the assignment of certain spectral features to the cysteine protons is in progress.

CONCLUSION

In this paper we presented the theory and experimental implementation of the refocused primary ESEEM, which, being formally introduced earlier by Grupp *et al.* (*12*) as a zero dead time variety of the primary ESE, now virtually emerges as a new 2D ESEEM technique. This method introduces correlations between various modulation harmonics, thus improving the informativity of the conventional primary ESEEM. We also found that integration of 2D time-domain data along one time coordinate produces spectra with a nonlinear response to the modulation amplitude factor k, which is used for substantial suppression of the sum combination line of weakly coupled protons. We demonstrated that this property of RP ESEEM combined with elimination of the dead time and with adjustment of the modulation amplitude by means of variation of the operational frequency is very useful for detection of weak and broad lines of close protons featuring strong and, possibly, distributed anisotropic hfi. This technique is practical to apply for solving structural problems related to the close ligand protons in metalloenzymes that are not demanding in spectral resolution, but require a substantial suppression of proton background lines arising from the protein backbone.

APPENDIX

1. *Shapes of the (α, σ), (β, σ), (σ, α), and (σ, β) Correlation Lines*

The (α, σ) and (β, σ) harmonics in Fig. 4 have a greater intensity toward the high-frequency end of the ν_α and ν_β lines, respectively. To understand this, we have to take into account that one of the factors influencing the amplitude of, e.g., the (α, σ) correlation line is the value of the derivative $\partial\nu_\alpha/\partial\nu_\sigma$. It has been shown (*1*) that

$$\nu_\sigma \approx 2\nu_I + B^2/4\nu_I, \qquad \text{[A1.1]}$$

where $B^2 = T_{ZX}^2 + T_{ZY}^2$. Using Eq. [A1.1], we can derive

$$\partial\nu_\alpha/\partial\nu_\sigma \propto \partial\nu_\alpha/\partial(B^2) \propto [1 + \text{sign}(T_\perp)\text{sign}(\theta - \pi/4) \times (2\nu_I + T_\perp/2)/(9T_\perp^2/4 - B^2)^{1/2}]/\nu_\alpha, \qquad \text{[A1.2]}$$

where $\theta \in [0, \pi/2]$ is the angle between the main axis of the axial hfi tensor and the direction of the static magnetic field $\mathbf{B}_0$. Equation [A1.1] shows that $|\partial\nu_\alpha/\partial\nu_\sigma|$ is minimal at $B^2 = 0$, which correspond to $\theta = 0$ and $\pi/2$. Of these two minima, the one corresponding to the greater ν_α is deeper, which results in an enhancement of the (α, σ) correlation line toward the high-frequency end of the anisotropic ν_α transition as observed in Fig. 4. Similar considerations apply to the (β, σ) correlation line.

2. *Self-suppression Effect for Broad Correlation Lines*

Let us model a modulation harmonic corresponding to a two-frequency correlation by an exponentially damping cosine function,

$$U(\tau, T) = \exp[-\alpha(\tau + T)]\cos(\omega_\tau\tau + \omega_T T), \qquad \text{[A2.1]}$$

where α describes the damping of the harmonic, for simplicity taken similar in the τ and T manifolds. Fourier transforming $U(\tau, T)$, we obtain

$$\text{Re}[U_{FT}(\omega, \omega')] \propto \frac{1 - (\omega_\tau - \omega)(\omega_T - \omega')/\alpha^2}{[1 + (\omega_\tau - \omega)^2/\alpha^2][1 + (\omega_T - \omega')^2/\alpha^2]}$$

$$\text{Im}[U_{FT}(\omega, \omega')] \propto \frac{(\omega_\tau - \omega + \omega_T - \omega')/\alpha}{[1 + (\omega_\tau - \omega)^2/\alpha^2][1 + (\omega_T - \omega')^2/\alpha^2]}, \qquad \text{[A2.2]}$$

where $\omega = 2\pi\nu$ and $\omega' = 2\pi\nu'$ are the frequencies corresponding to the τ and T manifolds, respectively. The integration over τ and T is performed in the limits from 0 to $+\infty$.

Equation [A2.2] describes the line centered at (ω_τ, ω_T), with the Lorentzian shape of the slices along ω at $\omega' = \omega_T$ and along ω' at $\omega = \omega_\tau$. We will be interested, however, in the shape of the slices along the diagonal ($\Delta\omega = \Delta\omega'$) and antidiagonal ($\Delta\omega = -\Delta\omega'$) of the 2D spectrum. To avoid confusion, note that under Theory the antidiagonal $\omega = -\omega'$ in the ($-+$) quadrant of the 2D spectrum was referred to as a main diagonal of that quadrant.

Let us consider the diagonal slice with $\omega = \omega_\tau + \delta\omega$ and $\omega' = \omega_T + \delta\omega$, where $\delta\omega$ is a frequency offset along the diagonal from the line maximum. Equation [A2.2] then reduces to

$$\text{Re}[U_{FT}(\delta\omega)] \propto \frac{1 - (\delta\omega/\alpha)^2}{[1 + (\delta\omega/\alpha)^2]^2}$$

$$\text{Im}[U_{FT}(\delta\omega)] \propto \frac{\delta\omega/\alpha}{[1 + (\delta\omega/\alpha)^2]^2}. \qquad \text{[A2.3]}$$

Equation [A2.3] shows that the real part of the diagonal slice has a positive (as we assumed the amplitude of the modulation harmonic in Eq. [A2.1] to be positive) maximum and negative wings. The sign change occurs at $|\delta\omega| = \alpha$ and the maximum negative amplitude attained in the wings at $|\delta\omega| = \sqrt{3}\alpha$ is $-\frac{1}{8}$.

As an example, Figs. A1c and A1d show, respectively, the real and imaginary parts of the ($++$) quadrant of the 2D spectrum calculated for $\nu_\tau = \omega_\nu/2\pi = 8$ MHz, $\nu_T = \omega_T/2\pi = 12$ MHz, and $\alpha = 2\ \mu s^{-1}$. The solid lines in Figs. A1a and A1b represent the diagonal slices of the 2D spectrum along solid straight lines in Figs. A1c and A1d. These lineshapes are described by Eq. [A2.3]. The calibration of the ν axis corresponding to this calculation is shown at the bottom of each panel in Fig. A1.

The above calculation was performed with sampling time intervals $\Delta\tau$ and ΔT equal to 0.02 μs, resulting in the Nyquist frequency of 25 MHz. The calculation with $\nu_\tau = -17$ MHz, $\nu_T = 12$ MHz, and $\alpha = 2\ \mu s^{-1}$ and with similar sampling intervals results in the ($-+$) quadrant of the 2D spectrum being identical to the ($++$) quadrant of the spectrum described above. Therefore, Fig. A1 also corresponds to the ($-+$) quadrant of the spectrum obtained in the second calculation and its diagonal and antidiagonal projections. The calibration of the ν axis corresponding to the second calculation is shown at the top of each panel in Fig. A1.

The amplitude in the wings of $\text{Re}[U_{FT}(\delta\omega)]$ is damping relatively slowly, leading to

$$\int_{-\infty}^{\infty} \text{Re}[U_{FT}(\delta\omega)]d(\delta\omega) = 0. \qquad \text{[A2.4]}$$

The integral of $\text{Im}[U_{FT}]$ equals zero because this function is antisymmetric with respect to $\delta\omega$. These integral properties of U_{FT} have interesting consequences. If an anisotropic line is

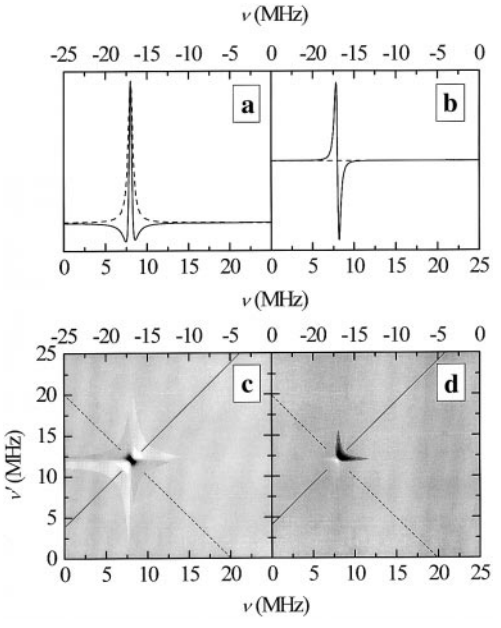

FIG. A1. The spectra of the exponentially damping harmonic described by Eq. [A2.1]. This figure simultaneously corresponds to two different calculations, one with $\nu_\tau = 8$ MHz, and the other one with $\nu_\tau = -17$ MHz. In both calculations $\nu_T = 12$ MHz, $\alpha = 2\ \mu s^{-1}$, and $\Delta\tau = \Delta T = 0.02\ \mu s$. In the case of the first calculation panels (c) and (d) represent, respectively, the real and imaginary parts of the $(++)$ quadrant of the 2D spectrum. In the case of the second calculation, these panels correspond to the $(-+)$ quadrant. Panels (a) and (b) show the diagonal (solid traces) and antidiagonal (dashed traces) slices of the spectra in panels (c) and (d), respectively. The diagonals and antidiagonals, along which the slices are taken, are shown in panels (c) and (d) by solid and dashed lines, respectively. The ν-axis calibrations shown at the bottom of each panel correspond to the first calculation (with $\nu_\tau = 8$ MHz). The ν-axis calibrations shown at the top of each panel correspond to the second calculation (with $\nu_\tau = -17$ MHz).

extended along the spectrum diagonal over a considerable frequency range, we may consider it to consist of an infinite number of infinitely closely situated "sublines" corresponding to different orientations of a paramagnetic center. The individual shapes of all the "sublines" (Eq. [A2.3]) add up in such a way as to diminish the inner part of the anisotropic line. The anisotropic line thus suppresses itself. This effect explains the small amplitude of the (α, α) and (β, β) harmonics in RP and 2D-CP ESEEM spectra. It also shows that one can hardly expect to detect a broad (σ, σ) line in the case of distributed anisotropic hfi.

For the antidiagonal slice with $\omega = \omega_\tau - \delta\omega$ and $\omega' = \omega_T + \delta\omega$, we obtain

$$\mathrm{Re}[U_{\mathrm{FT}}(\delta\omega)] \propto \frac{1 + (\delta\omega/\alpha)^2}{[1 + (\delta\omega/\alpha)^2]^2} = \frac{1}{1 + (\delta\omega/\alpha)^2}, \quad [A2.5]$$

i.e., a Lorentzian damping without any sign changes. At the same time, for the antidiagonal slice, $\mathrm{Im}[U_{\mathrm{FT}}(\delta\omega)] = 0$. Therefore, if the anisotropic line extends along the antidiagonal (like (α, β) and (β, α) correlation lines), its amplitude is not suppressed.

ACKNOWLEDGMENTS

The authors are grateful to Drs. J. H. Enemark and A. Pacheco for supplying us with a sample of chicken liver sulfite oxidase and for helpful discussions on its structure, and to Dr. V. Kozliouk for useful discussions of the technical problems related to our experiments. The financial support of NSF DBI-9604939 (to Drs. A. Raitsimring and F. A. Walker) for construction of the pulsed EPR spectrometer is gratefully acknowledged. Dr. A. Astashkin is thankful to NIH DK 31038 (to Dr. F. A. Walker) for financial support of the research presented herein.

REFERENCES

1. A. V. Astashkin, S. A. Dikanov, and Yu. D. Tsvetkov, *Chem. Phys. Lett.* **136,** 204 (1987).
2. J. L. Davis and W. B. Mims, *Rev. Sci. Instrum.* **52,** 131 (1981).
3. P. A. Narayana, R. J. Massoth, and L. Kevan, *Rev. Sci. Instrum.* **53,** 624 (1983).
4. W. B. Mims, *J. Magn. Reson.* **59,** 291 (1984).
5. A. Schweiger and R. R. Ernst, *J. Magn. Reson.* **77,** 512 (1988).
6. P. P. Borbat, R. H. Crepeau, and J. H. Freed, *J. Magn. Reson.* **127,** 155 (1997).
7. H. Cho, S. Phenninger, C. Gemperle, A. Schweiger, and R. R. Ernst, *Chem. Phys. Lett.* **160,** 391 (1989).
8. P. Höfer, *J. Magn. Reson. A* **116,** 221 (1995).
9. S. Van Doorslaer and A. Schweiger, *Chem. Phys. Lett.* **281,** 297 (1997).
10. A. V. Astashkin, A. Kawamori, Y. Kodera, S. Kuroiwa, and K. Akabori, *J. Chem. Phys.* **102,** 5583 (1995).
11. P. E. Doan and B. M. Hoffman, *Chem. Phys. Lett.* **269,** 208 (1997).
12. A. Grupp, Z. Shanmin, and M. Mehring, Deadtime free echo modulation in pulsed EPR, *in* "Congress Ampere on Magnetic Resonance and Related Phenomena, Extended Abstracts, Stuttgart 1990" (M. Mehring, J. U. von Schütz, and H. C. Wolf, Eds.), p. 454, Springer-Verlag, Berlin (1990).
13. C. Gemperle, G. Aebli, A. Schweiger, and R. R. Ernst, *J. Magn. Reson.* **88,** 241 (1990).
14. A. Pacheco, P. Basu, P. Borbat, A. M. Raitsimring, and J. H. Enemark, *Inorg. Chem.* **35,** 7001 (1996).
15. A. V. Astashkin, V. Kozlyuk, and A. M. Raitsimring, *in* Abstracts of the 40th Rocky Mountain Conference on Analytical Chemistry, Denver, CO, July 26–30 (1998). Additional materials.
16. W. B. Mims, *Phys. Rev. B* **5,** 2409 (1972).
17. A. Bloom, *Phys. Rev.* **98,** 1105 (1955).
18. A. V. Astashkin and A. M. Raitsimring, Optimization of the ESEEM acquisition using high-speed digitizing technique, *in* Abstracts of the 41st Rocky Mountain Conference on Analytical Chemistry, Denver, CO, August 1–5 (1999), p. 69.
19. S. A. Dikanov, A. V. Astashkin, and Yu. D. Tsvetkov, *Chem. Phys. Lett.* **144,** 251 (1988).
20. A. M. Raitsimring, A. Pacheco, and J. H. Enemark, *J. Am. Chem. Soc.* **120,** 11263 (1998).
21. C. Kisker, H. Schindelin, A. Pacheco, W. Wehbi, R. M. Garret, K. V. Rajagopalan, J. H. Enemark, and D. C. Rees, *Cell* **91,** 973 (1997).